photonics

Communication

# The Evolution Characteristics of Twisted Hermite–Gaussian Schell-Model Beams Propagating in a Uniaxial Crystal

**Rong Lin [1,2], Hongyan Sun [1], Hui Zhang [2,3], Yonglei Liu [2,3], Jidong Wu [2,3], Jiayi Yu [2,3], Yangjian Cai [2,3,*] and Xinlei Zhu [2,3,*]**

1 College of Physics and Electronic Engineering, Heze University, Heze 274015, China; linrong@hezeu.edu.cn (R.L.); sunhongyan@hezeu.edu.cn (H.S.)
2 Collaborative Innovation Center of Light Manipulation and Applications, Shandong Normal University, Jinan 250358, China; 2020010068@stu.sdnu.edu.cn (H.Z.); 2017020881@stu.sdnu.edu.cn (Y.L.); 2022010104@stu.sdnu.edu.cn (J.W.); jiayiyu0528@sdnu.edu.cn (J.Y.)
3 Shandong Provincial Engineering and Technical Center of Light Manipulations & Shandong Provincial Key Laboratory of Optics and Photonic Devices, School of Physics and Electronics, Shandong Normal University, Jinan 250014, China
* Correspondence: yangjiancai@sdnu.edu.cn (Y.C.); zhuxinleiphy@sdnu.edu.cn (X.Z.)

**Abstract:** In this paper, we study the propagation properties of twisted Hermite–Gaussian Schell-model (THGSM) beams propagating in a uniaxial crystal orthogonal to the optical axis. We derive the concrete analytical expression of the cross-spectral density (CSD) function in the crystal and simulate the evolution characteristics of such beams, including normalized spectral intensity, the spectral degree of coherence (DOC), and effective beam width. We find that the spectral intensity distribution exhibits a non-circular symmetric self-splitting while rotating, and the distribution of the spectral DOC is non-circular symmetric rotationally distorted, which is quite different from that in an isotropic medium. The initial beam parameters and crystal parameters both affect the distribution of spectral intensity and DOC. Furthermore, increasing the twist factor and adjusting the ratio of the extraordinary light refractive index and the ordinary light refractive index $n_e/n_o$ of the uniaxial crystal can suppress the beam expansion as propagating in the crystal. Our results show that the uniaxial crystal can be used to determine whether light beams carry a twist phase or not, and to modulate the characteristics of light beams.

**Keywords:** twisted Hermite–Gaussian Schell-model beams; uniaxial crystal; propagation



**Citation:** Lin, R.; Sun, H.; Zhang, H.; Liu, Y.; Wu, J.; Yu, J.; Cai, Y.; Zhu, X. The Evolution Characteristics of Twisted Hermite–Gaussian Schell-Model Beams Propagating in a Uniaxial Crystal. *Photonics* **2023**, *10*, 507. https://doi.org/10.3390/photonics10050507

Received: 23 March 2023
Revised: 24 April 2023
Accepted: 25 April 2023
Published: 27 April 2023



## 1. Introduction

As they have numerous practical merits respective to laser beams, partially coherent beams have been widely studied in all areas of the optical field in recent decades, such as remote sensing, imaging, free-space optical communications, encryption [1–5], etc. Originally, most of the studies mentioned above were concentrated on conventional Gaussian Schell-model (GSM) beams. Until Gori and co-workers found the necessary conditions for constructing genuine correlation functions of partially coherent beams with special correlated structure [6,7], it garnered wide attention in the optical field, and a variety of special correlation partially coherent beams have been introduced [8–11]. Especially in recent years, various special correlation partially coherent beams have been studied in detail and their distinctive transmission properties that are superior to those of conventional GSM beams have been excavated out. For instance, the multi-Gaussian Schell model beams and Laguerre–Gaussian correlated Schell-model beams can realize self-shape in the far field [8,9]. Hermite–Gaussian correlated Schell-model beams can realize self-splitting [10]. Since the discovery of non-uniform correlated beams [11], their research has received widespread attention, especially in recent years, and has shown that the non-uniformly correlated beam can realize self-focusing and self-shifting [12], and the optical coherence lattices [13] which can be used to generate far-field arrays of structured random beams [14] can realize the periodicity reciprocity [15]. Twisted Hermite–Gaussian Schell model (THGSM) beams have been introduced [16] and generated experimentally [17], and it has been revealed that THGSM beams have many superior properties relative to other partially coherent beams. For example, it can realize the adjustment of the number of light spots at the source plane, and the THGSM beams simultaneously possess self-splitting and rotation properties, and it can also maintain these characteristics when it propagates in turbulence. In addition to the above points, it also has several degrees of freedom that can be regulated to change the orbital angular momentum and optimize diverse turbulent circumstances. Therefore, THGSM beams are an outstanding expectant for use in physical applications in challenging media. It is natural to study whether THGSM beams can maintain these characteristics when they propagate in an anisotropic medium.

As an anisotropic medium, uniaxial crystals are widely used in optical systems and optical devices such as laser resonators owing to their excellent optical and physical properties. In fact, with the wide applications of uniaxial crystals, up to now, the evolutionary characteristics of many kinds of beams including coherent beams [18–22] and traditionally correlated partially coherent beams [23–27] propagating in uniaxial crystals have been widely studied. Right after, the evolution properties of scalar and vector Laguerre–Gaussian correlated Schell-model beams propagating in uniaxial crystals were also reported [28,29]. The evolution properties of rectangular Hermite non-uniformly correlated beams propagating in uniaxial crystals were studied [30], and interestingly, it was found that the crystal refractive index can be measured by using the self-focusing properties of such beams, which opens the door to the application of partially coherent beams in the field of crystal measurement. This further leads researchers to think about the propagation characteristics of partially coherent beams in uniaxial crystals.

In this paper, we studied the propagation properties of THGSM beams propagating in a uniaxial crystal and the beam propagation direction is orthogonal to that of the optical axis. It finds that THGSM beams can also maintain self-splitting and rotating when propagating in uniaxial crystals, and the spectral intensity distribution exhibits a non-circular symmetric self-splitting while rotating, and the distribution of the spectral DOC is a non-circular symmetric rotationally distorted, which is quite different from that in isotropic media. In addition, the evolution of the effective beam width of THGSM beams is also studied, and it finds the twist factor can reduce beam divergence.

## 2. The Cross-Spectral Density Function of THGSM Beams Propagating in Uniaxial Crystals Orthogonal to the Optical Axis

Here, we begin to research the paraxial propagation characteristic of THGSM beams propagating in a uniaxial crystal. Our discussions in this paper are all based on the following conditions, that THGSM beams propagate along the $z$-axis direction in the crystal and the optical axis of the crystal is along the x-axis. The dielectric tensor of the uniaxial crystal can be shown as:

$$\varepsilon = \begin{bmatrix} n_e^2 & 0 & 0 \\ 0 & n_0^2 & 0 \\ 0 & 0 & n_0^2 \end{bmatrix} \tag{1}$$

where $n_e$ and $n_o$ are, respectively, the extraordinary refractive indices and ordinary refractive indices. In the paraxial approximation, the transverse components of the electric field that propagate in the uniaxial crystal can be calculated through the following expressions [31]:

$$\boldsymbol{E}_x(\rho_x, \rho_y, z) = \exp(ikn_e z)\frac{kn_o}{2\pi iz}\int \exp\left\{-\frac{k}{2izn_e}\left[n_o^2(\rho_x - x)^2 + n_e^2(\rho_y - y)^2\right]\right\}\boldsymbol{E}_x(x, y, 0)dxdy, \tag{2}$$

$$\boldsymbol{E}_y(\rho_x, \rho_y, z) = \exp(ikn_o z)\frac{kn_o}{2\pi iz}\int \exp\left\{-\frac{kn_o}{2iz}\left[(\rho_x - x)^2 + (\rho_y - y)^2\right]\right\}\boldsymbol{E}_y(x, y, 0)dxdy, \tag{3}$$

where $\boldsymbol{E}_{x,y}(\rho_x, \rho_y, z)$ and $\boldsymbol{E}_{x,y}(x,y,0)$ are the $x$ and $y$ component of the electric fields in the output plane and the input plane, respectively, $k = 2\pi/\lambda$ means the wave number, and $\lambda$ means the wavelength.

It can be obtained from Equations (2) and (3) that the expression of the $y$ component conforms to the Fresnel diffraction of paraxial transmission in an isotropic medium, but the $x$ component undergoes a diffraction-spreading asymmetry along and orthogonal to the optical axis direction. Therefore, only the $x$ linearly polarized THGSM beams propagating in uniaxial crystals orthogonal to the optical axis are considered in our work, and $E_y(\rho_x, \rho_y) = 0$

For partially coherent beams, in the space–frequency domain, the second-order coherence properties are usually characterized by the cross-spectral density (CSD) function which is defined as a two-point correlation function:

$$W(\boldsymbol{r}_1, \boldsymbol{r}_2) = \langle E^*(\boldsymbol{r}_1) E(\boldsymbol{r}_2) \rangle, \tag{4}$$

where ***E(r)*** denotes the field realization in a transverse plane that is perpendicular to the $z$-axis, $\boldsymbol{r}_1 = (x_1, y_1)$ and $\boldsymbol{r}_2 = (x_2, y_2)$ are two arbitrary position vectors in the transverse plane, the asterisk indicates the complex conjugate, and the angular brackets mean an average over an ensemble of monochromatic field realizations.

For THGSM beams, the CSD in the source plane can be expressed as [10]:

$$\begin{aligned} W(\boldsymbol{r}_1, \boldsymbol{r}_2) = \; & \exp\left(-\frac{\boldsymbol{r}_1^2 + \boldsymbol{r}_2^2}{4\omega_0^2}\right) \exp\left[-\frac{(\boldsymbol{r}_1 - \boldsymbol{r}_2)^2}{2\delta_g^2}\right] H_{2m}\left[\frac{1}{2\sqrt{\alpha}}(x_1 - x_2) + \frac{iu\sqrt{\alpha}}{2}(y_1 + y_2)\right] \\ & \times H_{2m}\left[\frac{1}{2\sqrt{\alpha}}(y_1 - y_2) - \frac{iu\sqrt{\alpha}}{2}(x_1 + x_2)\right] \exp[-iu(x_1 y_2 - x_2 y_1)], \end{aligned} \tag{5}$$

where $\omega_0 = (4\sigma - 2\alpha u^2)^{-1/2}$ is the beam width parameters, $\delta g = \sqrt{2}(1/\alpha + \alpha u^2)^{-1/2}$ is transverse coherence width, $\sigma$ is a positive real constant characterizing the width of the kernel function, $\alpha$ is a positive constant, $u$ is the twist factor, $H_{2m}[\ ]$ is the Hermite polynomial of order, and $m$ is the beam order.

This assumes that THGSM beams are incident on the uniaxial crystal in the $z = 0$ plane, and through Equations (2)–(4), we can obtain the CSD of THGSM beams at the arbitrary transmission distance $z$ in a uniaxial crystal:

$$\begin{aligned} W(\boldsymbol{\rho}_1, \boldsymbol{\rho}_2) = \; & \frac{k^2 n_o^2}{4\pi^2 z^2} \iint W(\boldsymbol{r}_1, \boldsymbol{r}_2) \exp\left\{-\frac{ik}{2zn_e}\left[n_o^2 (x_1 - \rho_{1x})^2 + n_e^2 (y_1 - \rho_{1y})^2\right]\right\} \\ & \times \exp\left\{\frac{ik}{2zn_e}\left[n_o^2 (x_2 - \rho_{2x})^2 + n_e^2 (y_2 - \rho_{2y})^2\right]\right\} d^2\boldsymbol{r}_1 d^2\boldsymbol{r}_2, \end{aligned} \tag{6}$$

where $W(\boldsymbol{r}_1, \boldsymbol{r}_2)$ and $W(\boldsymbol{\rho}_1, \boldsymbol{\rho}_2)$ are the CSD of THGSM beams at the source plane and output plane, respectively, and it can be calculated by using Formula (5), and the result is as follows:

$$\begin{aligned} W(\boldsymbol{\rho}_1, \boldsymbol{\rho}_2) = \; & C_0 \exp\left[-\frac{ik\left(n_o^2 \rho_{1x}^2 + n_e^2 \rho_{1y}^2\right)}{2zn_e} + \frac{ik\left(n_o^2 \rho_{2x}^2 + n_e^2 \rho_{2y}^2\right)}{2zn_e}\right] \exp\left(\frac{H_1^2}{J_1} + \frac{Q_2^2}{J_2}\right) \\ & \times \exp\left[-\frac{\sigma k^2 n_o^4 \left(\rho_{1x}^2 + \rho_{2x}^2\right)}{4z^2 n_e^2 \sigma^2 + k^2 n_o^4} - \frac{\sigma k^2 n_e^4 \left(\rho_{1y}^2 + \rho_{2y}^2\right)}{4z^2 n_e^2 \sigma^2 + k^2 n_e^4}\right] \\ & \times \exp\left[\frac{ik^3 n_o^6 \left(\rho_{1x}^2 - \rho_{2x}^2\right)}{2zn_e\left(4z^2 n_e^2 \sigma^2 + k^2 n_o^4\right)} + \frac{ik^3 n_e^6 \left(\rho_{1y}^2 - \rho_{2y}^2\right)}{2zn_e\left(4z^2 n_e^2 \sigma^2 + k^2 n_e^4\right)}\right], \end{aligned} \tag{7}$$

where the parameters in the formula are as follows:

$$J_1 = \alpha + \frac{2z^2 n_e^2 \sigma}{4z^2 n_e^2 \sigma^2 + k^2 n_o^4} - \frac{2z^2 n_e^2 \sigma \alpha^2 u^2}{4z^2 n_e^2 \sigma^2 + k^2 n_e^4}, \tag{8}$$

$$G_1 = \frac{zn_e k n_o^2 \alpha u}{4z^2 n_e^2 \sigma^2 + k^2 n_o^4} - \frac{zn_e k n_e^2 \alpha u}{4z^2 n_e^2 \sigma^2 + k^2 n_e^4}, \tag{9}$$

$$G_2 = \alpha + \frac{2z^2 n_e^2 \sigma}{4z^2 n_e^2 \sigma^2 + k^2 n_e^4} - \frac{2z^2 n_e^2 \sigma \alpha^2 u^2}{4z^2 n_e^2 \sigma^2 + k^2 n_o^4}, \tag{10}$$

$$\begin{aligned} H_1 = \; & \frac{ik^2 n_o^4 (\rho_{1x} - \rho_{2x}) - 2zn_e k n_o^2 (\rho_{1x} + \rho_{2x})\sigma}{2(4z^2 n_e^2 \sigma^2 + k^2 n_o^4)} \\ & - \frac{k^2 n_e^4 (\rho_{1y} + \rho_{2y})\alpha u + i2zkn_e^3 (\rho_{1y} - \rho_{2y})\sigma \alpha u}{2(4z^2 n_e^2 \sigma^2 + k^2 n_e^4)}, \end{aligned} \tag{11}$$

$$\begin{aligned} H_2 = \; & \frac{k^2 n_o^4 (\rho_{1x} + \rho_{2x})\alpha u + 2i\sigma \alpha u z n_e k n_o^2 (\rho_{1x} - \rho_{2x})}{2\left(4z^2 n_e^2 \sigma^2 + k^2 n_o^4\right)} \\ & + \frac{ik^2 n_e^4 \left(\rho_{1y} - \rho_{2y}\right) - 2zn_e k n_e^2 \left(\rho_{1y} + \rho_{2y}\right)\sigma}{2\left(4z^2 n_e^2 \sigma^2 + k^2 n_e^4\right)}, \end{aligned} \tag{12}$$

$$J_2 = G_2 - \frac{G_1^2}{J_1}, \tag{13}$$

$$Q_2 = H_2 + \frac{G_1 H_1}{J_1}, \tag{14}$$

$$\begin{aligned} C_0 = \; & \frac{4^{2m} k^2 n_o^2 n_e^2 \alpha^{2m+1} (2m)!}{\sqrt{J_1}\sqrt{J_2}} \sqrt{\frac{1}{4z^2 n_e^2 \sigma^2 + k^2 n_o^4}} \sqrt{\frac{1}{4z^2 n_e^2 \sigma^2 + k^2 n_e^4}} \times \\ & \sum_{l=0}^{m} \sum_{f=0}^{2m-2l} \sum_{d=0}^{(4m-2l-f)/2} \begin{pmatrix} 2m-2l \\ f \end{pmatrix} \frac{(4m-2l-f)! G_1^{2m-2l-f} {H_1}^f Q_2^{4m-2l-f-2d}}{4^{l+d} (4m-2l-f-2d)! d! (2m-2l)! l! J_1^{2m-l} J_2^{4m-2l-f-d}}, \end{aligned} \tag{15}$$

The spectral intensity at any transmission plane in the crystal can be attained by making $\boldsymbol{\rho}_1 = \boldsymbol{\rho}_2 = \boldsymbol{\rho}$, that is [32]:

$$S(\boldsymbol{\rho}) = W(\boldsymbol{\rho}, \boldsymbol{\rho}), \tag{16}$$

Additionally, the DOC of THGSM beams at any two points is as follows [32]:

$$\mu(\boldsymbol{\rho}_1, \boldsymbol{\rho}_2) = \frac{W(\boldsymbol{\rho}_1, \boldsymbol{\rho}_2)}{\sqrt{W(\boldsymbol{\rho}_1, \boldsymbol{\rho}_1) W(\boldsymbol{\rho}_2, \boldsymbol{\rho}_2)}}, \tag{17}$$

## 3. The Propagation Characteristics of THGSM Beams Propagating in Uniaxial Crystal Orthogonal to the Optical Axis

Next, the evolutionary characteristics of the spectral intensity and the coherent structure of THGSM beams propagating in a uniaxial crystal are simulated and analyzed according to Equation (16) and Equation (17). In the following simulations, except for special instructions, the parameters take the following values λ = 632.8 nm, $\sigma = 5 \times 10^{-3} \mu m^{-2}$, $\alpha = 80\ \mu m^2$, and $n_o = 2.616$.

In order to study the effect of the parameters of crystal on the propagation properties of THGSM beams, the evolutionary characteristics of the density diagram of the normalized spectral intensity of THGSM beams propagating in different uniaxial crystals are given in Figure 1. Without losing generality, the beam order and twist factor here are $m = 1$, $u = 0.5 \times 10^{-2}\ \mu m^{-2}$, respectively. In order to compare the propagation characteristics with those in isotropic media and free space, the normalized spectral intensity of THGSM beams propagating in free space and in isotropic media has also been given in Figure 1.

From Figure 1, we know THGSM beams can realize rotation and splitting simultaneously when it propagates in uniaxial crystals as in the free space and in isotropic media. However, the needed propagation distances that it splits into four spots are different in different media. When it propagates in negative uniaxial crystals, the beam spot is elongated along the $y$ direction; it splits and rotates, as can be seen in Figure 1c1–c5. On the contrary, the spot is elongated in the $x$ direction when it propagates in a positive crystal, and the bigger the ratio, $n_e/n_o$, the greater the stretching degree, which can be seen by comparing line 4 and line 5 in Figure 1. This is mainly because, for anisotropic uniaxial crystals, the diffraction is anisotropic, and the diffraction characteristics have the largest difference between the $x$ direction and the $y$ direction. When the difference between the two main refractive indexes $n_e$ and $n_o$ is higher, the corresponding stretching degree is greater.

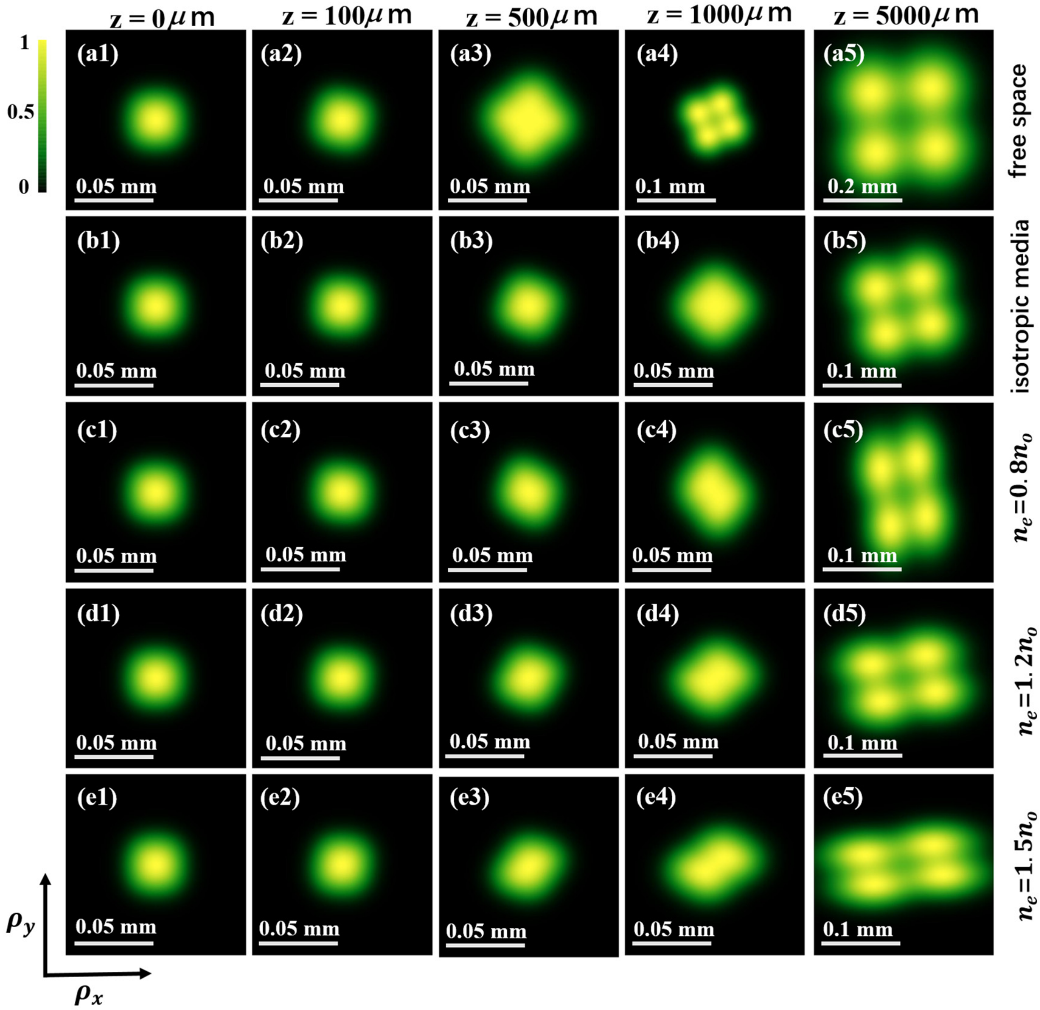


**Figure 1.** The evolutionary properties of the density diagram of the normalized spectral intensity of THGSM beams propagating (**a1**)–(**a5**) in the free space, (**b1**)–(**b5**) in the isotropic media, (**c1**)–(**c5**) in the uniaxial crystal, $n_e = 0.8n_o$, (**d1**)–(**d5**) in the uniaxial crystal, $n_e = 1.2n_o$, (**e1**)–(**e5**) in the uniaxial crystal, $n_e = 1.5n_o$, $n_o = 2.616$.

Figure 2 shows the effect of the twist factor on the evolutionary characteristic of THGSM beams propagating in uniaxial crystals. For the sake of generality, the beam order and crystal parameters in this figure are, respectively, $m = 1$, $n_o = 2.616$, and $n_e = 1.2n_o$. It shows that the beam spot rotates counterclockwise when the twist factor is negative, and it rotates clockwise when the twist factor is positive with the increase in the transmission distance. The pattern of the normalized spectral intensity splits more obviously and rotates more quickly when the twist factor is bigger which can be obtained by comparing line 2 and line 3 in Figure 2.

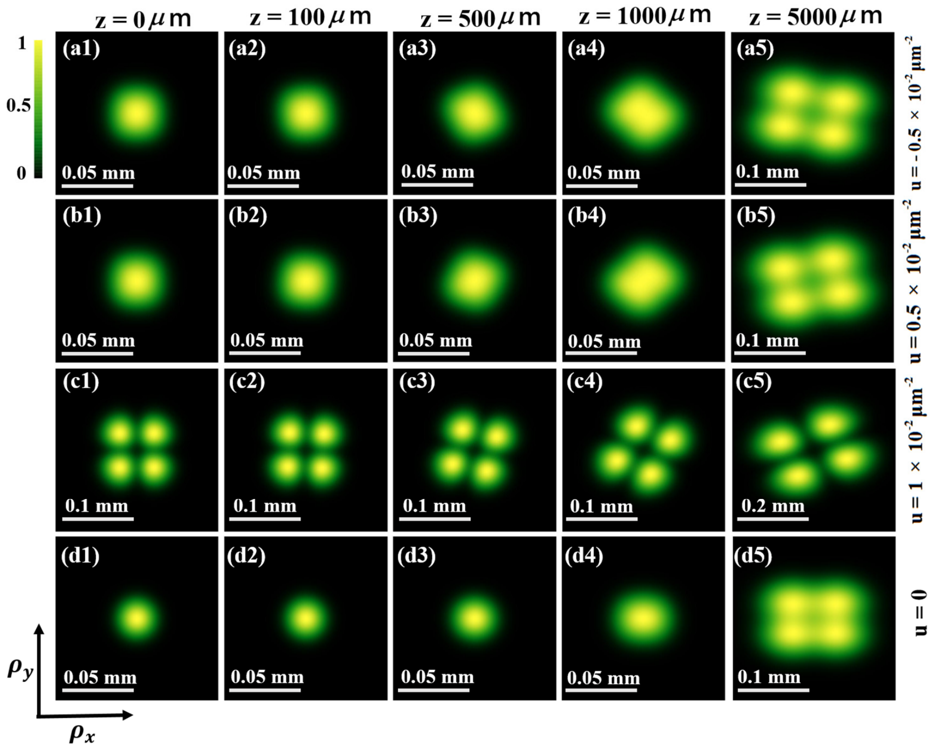


**Figure 2.** The evolutionary properties of the density diagram of the normalized spectral intensity of THGSM beams with different twist factors propagating in uniaxial crystal, (**a1**)–(**a5**) the twist factor $u = -0.5 \times 10^{-2} \mu\text{m}^{-2}$, (**b1**)–(**b5**) the twist factor $u = 0.5 \times 10^{-2}\ \mu\text{m}^{-2}$, (**c1**)–(**c5**) the twist factor $u = 1 \times 10^{-2}\ \mu\text{m}^{-2}$, (**d1**)–(**d5**) the twist factor $u = 0$.

Figure 3 shows the evolutionary characteristics of the normalized spectral intensity of THGSM beams with different beam orders propagating in uniaxial crystals. For universality, the beam twist factor and crystal parameter in this figure are $u = 0.5 \times 10^{-2}\ \mu\text{m}^{-2}$, $n_o = 2.616$, and $n_e = 1.2n_o$, respectively. It can be seen easily that the larger the beam order, the more obvious the spot splitting corresponding to the same transmission distance.

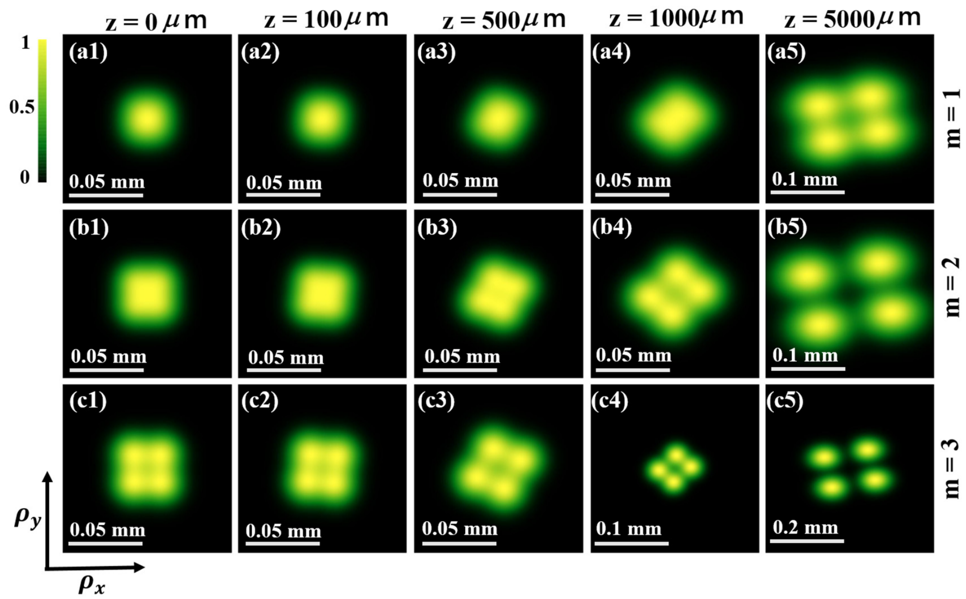


**Figure 3.** The evolutionary properties of the density diagram of the normalized spectral intensity of THGSM beams with different beam orders propagating in uniaxial crystal, (**a1**)–(**a5**) the beam order $m = 1$, (**b1**)–(**b5**) the beam order $m = 2$, (**c1**)–(**c5**) the beam order $m = 3$.

## 4. The Distribution of the DOC of THGSM Beams Propagating in Uniaxial Crystals Orthogonal to the Optical Axis

Then, we study the coherent structure of THGSM beams propagating in uniaxial crystals. The density diagrams of the absolute value of the DOC of THGSM beams propagating in uniaxial crystals are given in Figures 4–6. We choose the position vector $\boldsymbol{\rho}_2(\boldsymbol{r}_2) = 0$, so the DOC is a function of $\boldsymbol{\rho}_1(\boldsymbol{r}_1)$. In order to study the influence of crystal parameters on the DOC, Figure 4 gives the density diagram distribution of the absolute value of the DOC of THGSM beams propagating in different media.

In Figure 4, line 1 corresponds to the free space, and line 2 corresponds to the isotropic media, and other lines correspond to uniaxial the crystal. It can be seen that the patterns of the DOC of THGSM beams propagating in different media all rotate, and the central light spot and the four light spots outside the central beam spot are all connected together to form a whole with the increase in the propagation distance. With the continued increase, it is not distributed in a wind fire wheel shape at the longer propagation distance when THGSM beams propagate in the free space, which can be seen in Figure 4a1–a5, but it still contains the wind fire wheel shape at the longer distance in other media. It can be seen from Figure 4b1–b5 that the patterns of the DOC of THGSM beams are the same in both the $x$ direction and the $y$ direction when THGSM beams propagate in isotropic media. By comparing Figure 4c1–c5,d1–d5, we can know that the patterns of the DOC are stretched in the $y$ direction when THGSM beams propagate in a positive crystal, and the patterns are stretched in the $x$ direction when THGSM beams propagate in a negative crystal. It can also be seen by comparing the last two lines in Figure 4 that the level of stretch of the patterns of the DOC is greater when the refractive index ratio of extraordinary light and ordinary light is bigger. Therefore, the evolution properties of the patterns of the DOC are similar to that of the normalized intensity as a result of the diffraction being anisotropic in uniaxial crystal.

Figure 5 shows the density diagram distribution of the absolute value of the DOC of THGSM beams with different twist factors propagating in uniaxial crystal. For universality, the beam order and crystal parameter in this figure are $m = 1$, $n_o = 2.616$, and $n_e = 1.2n_o$. It can be concluded that the twist factor causes the density map distribution of the absolute value of the DOC to rotate during transmission. By comparing Figure 5a1–a5,b1–b5, it can be seen that the density diagram of the absolute value of the DOC of THGSM beams consists of five light spots when the twist factor is small. With the increase in the transmission distance, the central light spot and the four surrounding light spots rotate simultaneously. They rotate counterclockwise when the twist factor is negative, and they rotate clockwise when the twist factor is positive. Eventually, the four light spots are all connected with the central light spot to form a whole, and it is distributed in a wind fire wheel shape at the longer transmission distance. By comparing Figure 5b1–b5,c1–c5, it can be seen that when the twist factor is larger, four slightly bright spot lines appear outside the central bright spot, which are connected together in a square distribution and form four small hollow dark spots with the internal central bright spot. With the increasing of the transmission distance, the central spot and the outer slightly bright square spot rotate simultaneously, and the four small hollow dark spots are still clearly visible. For ease of comparison, the evolution of the density diagram of the absolute value of the DOC of Hermite–Gaussian Schell-mode beams propagating in the uniaxial crystal is shown in Figure 5d1–d5. It can be seen from Figure 5d1–d5 that the density diagram is composed of nine light spots at the input plane of the crystal, and then the external light spot gradually becomes blurred, and, finally, it is connected with the central light spot with the increase in the transmission distance, and the size of the light spot in the $x$ direction is larger than that in the $y$ direction (for the positive crystal).

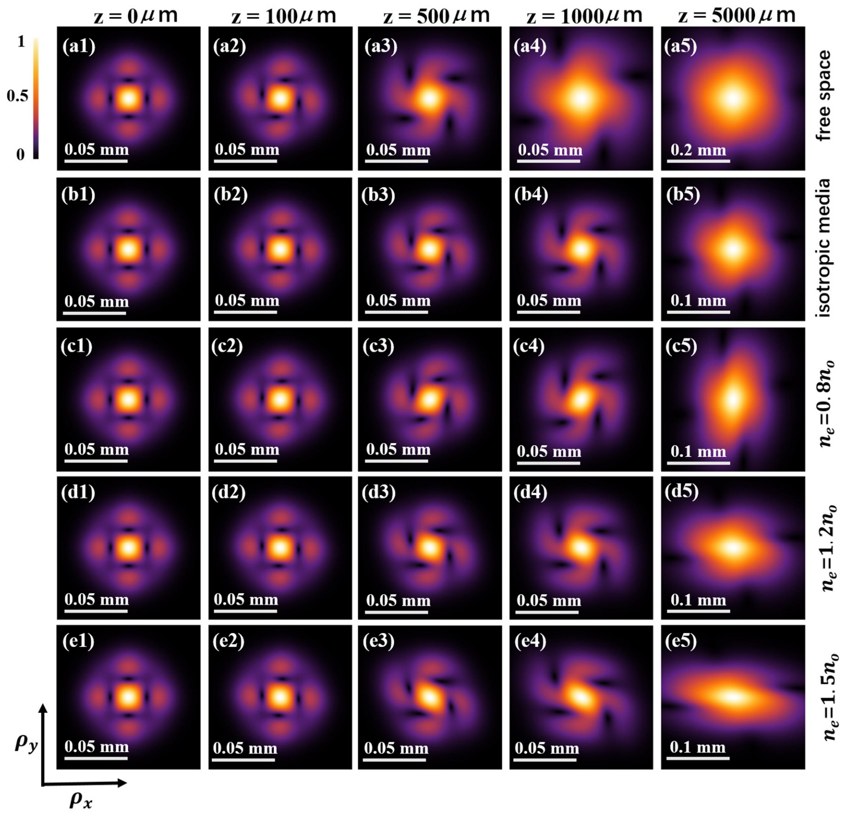


**Figure 4.** The evolutionary properties of the density diagram of the absolute value of the DOC of THGSM beams propagating (**a1**)–(**a5**) in the free space, (**b1**)–(**b5**) in the isotropic media, (**c1**)–(**c5**) in the uniaxial crystal, $n_e = 0.8n_o$, (**d1**)–(**d5**) in the uniaxial crystal, $n_e = 1.2n_o$, (**e1**)–(**e5**) in the uniaxial crystal, $n_e = 1.5n_o$. $m = 1$, $u = 0.5 \times 10^{-2}$ $\mu m^{-2}$, and $n_o = 2.616$.

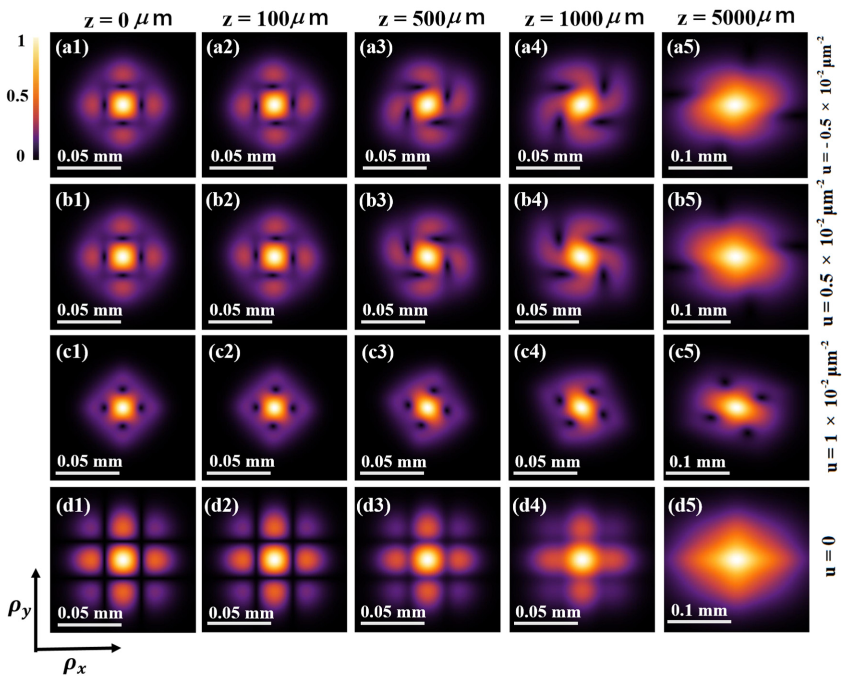


**Figure 5.** The evolutionary properties of the density diagram of the absolute value of the DOC of THGSM beams with different twist factors propagating in uniaxial crystal, (**a1**)–(**a5**) the twist factor $u = -0.5 \times 10^{-2} \mu m^{-2}$, (**b1**)–(**b5**) the twist factor $u = 0.5 \times 10^{-2}$ $\mu m^{-2}$, (**c1**)–(**c5**) the twist factor $u = 1 \times 10^{-2}$ $\mu m^{-2}$, (**d1**)–(**d5**) the twist factor $u = 0$.

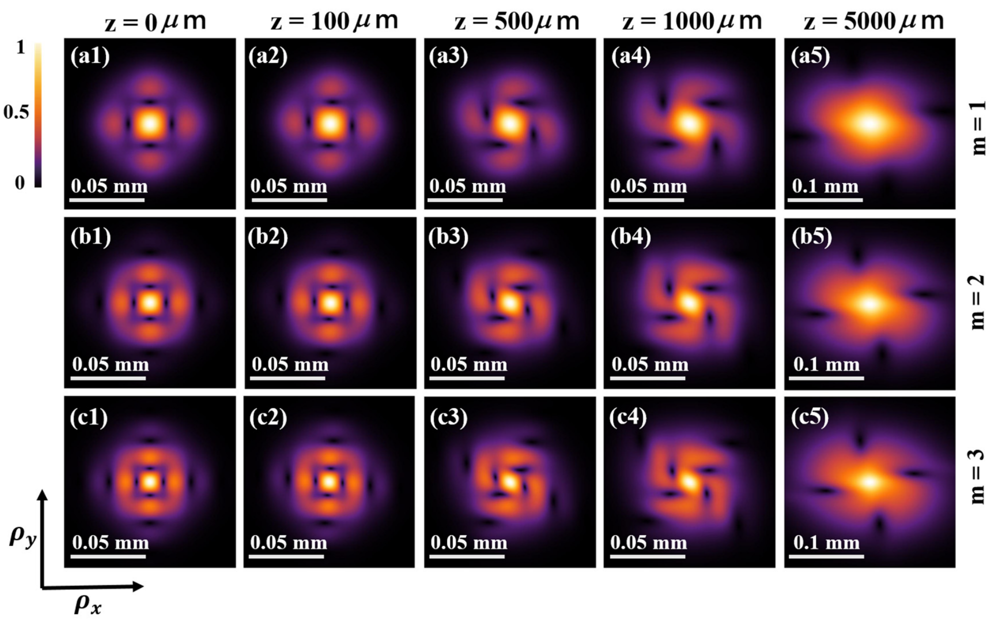


**Figure 6.** The evolutionary properties of the density diagram of the absolute value of the DOC of THGSM beams with different beam orders propagating in uniaxial crystal, (**a1**)–(**a5**) the beam order $m$ = 1, (**b1**)–(**b5**) the beam order $m$ = 2, (**c1**)–(**c5**) the beam order $m$ = 3.

Figure 6 shows the density diagram distribution of the absolute value of the DOC of THGSM beams with different beam orders propagating in a uniaxial crystal along the direction vertical to the optical axis. Additionally, the twist factor and crystal parameter are $u = 0.5 \times 10^{-2}$ μm$^{-2}$, $n_o = 2.616$, and $n_e = 1.2n_o$, respectively. It can be seen from Figure 6 that the density diagram distributions of the absolute value of the DOC of THGSM beams corresponding to different beam orders are different on the input plane of the crystal, and the density diagram rotates with the increase in the transmission distance. With the increase in the beam order, the number of side lobes outside the central beam spot in the density diagram increases, the central beam spot becomes small, the side lobes gradually connect together, and, finally, they all show a wind fire wheel distribution at a long transmission distance.

## 5. The Effective Beam Width of THGSM Beams Propagating in Uniaxial Crystal

In this part, we study the evolutionary characteristics of the effective beam width of THGSM beams propagating in uniaxial crystals. The effective beam width of the partially coherent beams at any propagation plane is defined as [33]:

$$W_s = \sqrt{\frac{2\int_{-\infty}^{\infty}\int_{-\infty}^{\infty} s^2 I(x,y,z)dxdy}{\int_{-\infty}^{\infty}\int_{-\infty}^{\infty} I(x,y,z)dxdy}} \quad (s = x,y), \tag{18}$$

where $W_x$ and $W_y$ are the effective beam widths along the $x$ direction and the $y$ direction. After a lengthy integration operation, the following quantities related to the effective beam width were acquired:

$$F_0 = \int_{-\infty}^{\infty}\int_{-\infty}^{\infty} I(x,y,z)dxdy = C_0\sum_{l=0}^{m}\sum_{f=0}^{2m-2l}\sum_{d=0}^{\frac{4m-2l-f}{2}}\sum_{p=0}^{f}\sum_{q=0}^{4m-2l-f-2d} Y_0 Y_{00} X_{00} X_1 X_2, \tag{19}$$

$$F_x = \int_{-\infty}^{\infty}\int_{-\infty}^{\infty} x^2 I(x,y,z)dxdy = C_0\sum_{l=0}^{m}\sum_{f=0}^{2m-2l}\sum_{d=0}^{\frac{4m-2l-f}{2}}\sum_{p=0}^{f}\sum_{q=0}^{4m-2l-f-2d} Y_0 Y_{01} X_{01} X_1 X_2, \tag{20}$$

$$F_y = \int_{-\infty}^{\infty}\int_{-\infty}^{\infty} y^2 I(x,y,z)dxdy = C_0 \sum_{l=0}^{m}\sum_{f=0}^{2m-2l}\sum_{d=0}^{\frac{4m-2l-f}{2}}\sum_{p=0}^{f}\sum_{q=0}^{4m-2l-f-2d} Y_0 Y_{00} X_{02} X_1 X_2, \quad (21)$$

Substituting Equations (19)–(21) into Equation (18), the effective spot widths in the $x$ direction and the $y$ direction of THGSM beams propagating in uniaxial crystals can be attained, respectively,

$$W_x = \sqrt{\frac{2F_x}{F_0}}, \quad (22)$$

$$W_y = \sqrt{\frac{2F_y}{F_0}}, \quad (23)$$

where the quantities in the formula are as follows:

$$C_1 = \frac{4^{2m}\sqrt{\pi}\alpha^{2m+1}(2m)!k^2 n_o^2 n_e^2}{\sqrt{J_1 J_2}\sqrt{M}} \sqrt{\frac{1}{4z^2 n_e^2\sigma^2 + k^2 n_o^4}} \sqrt{\frac{1}{4z^2 n_e^2\sigma^2 + k^2 n_e^4}}, \quad (24)$$

$$Y_0 = \frac{(4m-2l-f)!(-1)^f}{(2m-2l-f)!4^{l+d+s}q!d!l!p!s!(f-p)!(4m-2l-f-2d-q)!}, \quad (25)$$

$$X_1 = \frac{\left(A_3 - \frac{G_1}{J_1}A_2\right)^{4m-2l-f-2d-q}\left(-B_3 - \frac{G_1}{J_1}B_2\right)^q}{T^{2s} J_1^{2m-l} J_2^{4m-2l-f-d}}, \quad (26)$$

$$X_2 = G_1^{2m-2l-f} A_2^{f-p} M^s B_2^p, \quad (27)$$

$$X_{00} = \left(\frac{T}{M}\right)^{4m-2l-2d-q-p} \frac{1}{M_1{}^{2m-l-d-s+1/2}} \Gamma\left(\frac{4m-2l-2d-2s+1}{2}\right), \quad (28)$$

$$Y_{00} = \sum_{s=0}^{E((4m-2l-2d-q-p)/2)} \frac{(4m-2l-2d-q-p)!}{(4m-2l-2d-q-p-2s)!}, \quad (29)$$

$$X_{01} = \left(\frac{T}{M}\right)^{4m-2l-2d-q-p+2} \frac{1}{M_1{}^{2m-l-d-s+3/2}} \Gamma\left(\frac{4m-2l-2d-2s+3}{2}\right), \quad (30)$$

$$Y_{01} = \sum_{s=0}^{E((4m-2l-2d-q-p+2)/2)} \frac{(4m-2l-2d-q-p+2)!}{(4m-2l-2d-q-p-2s+2)!}, \quad (31)$$

$$X_{02} = \left(\frac{T}{M}\right)^{4m-2l-2d-q-p} \frac{1}{M_1{}^{2m-l-d-s+3/2}} \Gamma\left(\frac{4m-2l-2d-2s+3}{2}\right), \quad (32)$$

$$T = \frac{A_2 B_2}{J_1} + \frac{\left(A_3 - \frac{G_1}{J_1}A_2\right)\left(-B_3 - \frac{G_1}{J_1}B_2\right)}{J_2}, \quad (33)$$

$$M = A_1 - \frac{A_2^2}{J_1} - \frac{\left(A_3 - \frac{G_1}{J_1}A_2\right)^2}{J_2}; \;\; M_1 = B_1 - \frac{B_2^2}{J_1} - \frac{\left(-B_3 - \frac{G_1}{J_1}B_2\right)^2}{J_2} - \frac{T^2}{M}, \quad (34)$$

$$A_1 = \frac{2\sigma k^2 n_o^4}{4z^2 n_e^2\sigma^2 + k^2 n_o^4}; \;\; B_1 = \frac{2\sigma k^2 n_e^4}{4z^2 n_e^2\sigma^2 + k^2 n_e^4}, \quad (35)$$

$$A_2 = \frac{2\sigma k n_o^2 z n_e}{4z^2 n_e^2\sigma^2 + k^2 n_o^4}; \;\; B_2 = \frac{k^2 n_e^4 u\alpha}{4z^2 n_e^2\sigma^2 + k^2 n_e^4}, \quad (36)$$

$$A_3 = \frac{k^2 n_o^4 u\alpha}{4z^2 n_e^2 \sigma^2 + k^2 n_o^4}; \quad B_3 = \frac{2zkn_e^3\sigma}{4z^2 n_e^2 \sigma^2 + k^2 n_e^4}, \tag{37}$$

In the following, we simulate the evolutionary characteristics of the effective beam width $W_x$ and $W_y$ of THGSM beams propagating in uniaxial crystals. Unless otherwise specified, the crystal parameters and beam parameters take the following values without a loss of generality: $u = 0.5 \times 10^{-2}$ μm$^{-2}$, $m = 1$, $n_o = 2.616$, and $n_e = 1.2n_o$.

Figure 7 shows the evolutionary properties of the effective beam width $W_x$ and $W_y$ of THGSM beams propagating in uniaxial crystals, and the cases in free space and isotropic media have also been given for ease of comparison. By comparing Figure 7a,b, we can know that the value of the effective beam width $W_x$ is always equal to $W_y$ at the same propagation distance in both free space and isotropic crystals. Nevertheless, for the uniaxial crystals, the effective beam width in the two directions $W_x$ and $W_y$ according to the same propagation distance is different. For the negative uniaxial crystal, $W_x$ is smaller than $W_y$ according to the same propagation distance, which can be seen by comparing the blue line in Figure 7a,b, and the opposite is the case for the positive uniaxial crystal. For the positive uniaxial crystal, it can also be seen that the greater the ratio, $n_e/n_o$, the bigger the difference in $W_x$ and $W_y$ according to the same propagation distance. There is a big difference in Figure 7a,b, that is with the increasing of the ratio of $n_e/n_o$, the effective beam width $W_x$ enlarging, while $W_y$ declines corresponding to the same transmission distance for the positive uniaxial crystal (the green line and the magenta line in Figure 7a,b).

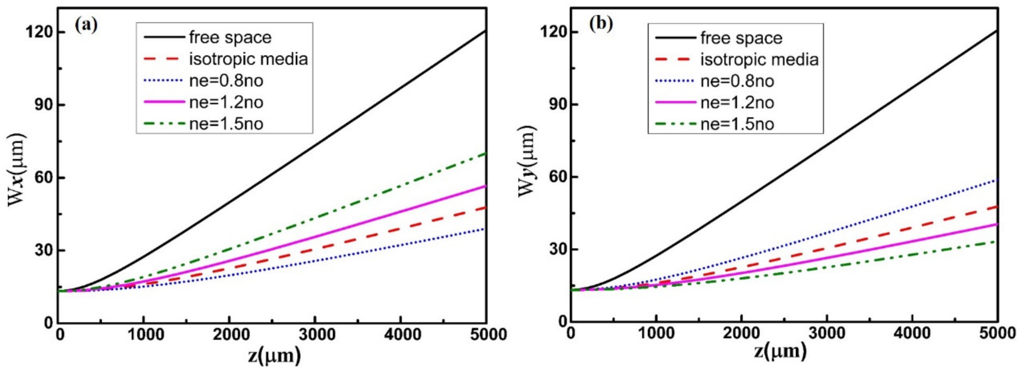


**Figure 7.** The evolutionary properties of (**a**) the effective beam width along the $x$ direction $W_x$, (**b**) the effective beam width along the $y$ direction $W_y$, of THGSM beams propagating in different media.

In order to seek out the influence of the twist factor on the evolutionary properties of the effective beam width $W_x$ and $W_y$, we further studied the evolutionary characteristics of the relative growth rate of the effective beam width, which is defined as follows:

$$\Delta W_x = \frac{W_x - W_{x0}}{W_{x0}}, \Delta W_y = \frac{W_y - W_{y0}}{W_{y0}}, \tag{38}$$

where $W_x$, $W_y$ are the effective beam width at any transmission distance and $W_{x0}$, $W_{y0}$ are the initial effective beam width along the $x$ direction and the $y$ direction.

As shown in Figure 8, the relative growth rate of $\Delta W_x$ and $\Delta W_y$ increase with the increase in the propagation distance whether the twist factor exists or not, and the relative growth rate of $\Delta W_x$ is bigger than that of $\Delta W_y$ at the same propagation distance corresponding to the same twist factor for the positive uniaxial crystal. It can also be seen that the relative growth rate of both $\Delta W_x$ and $\Delta W_y$ are lower when the twist factor is bigger, corresponding to the same propagation distance. Therefore, increasing the twist factor can further reduce the relative divergence rate of the beam radius.

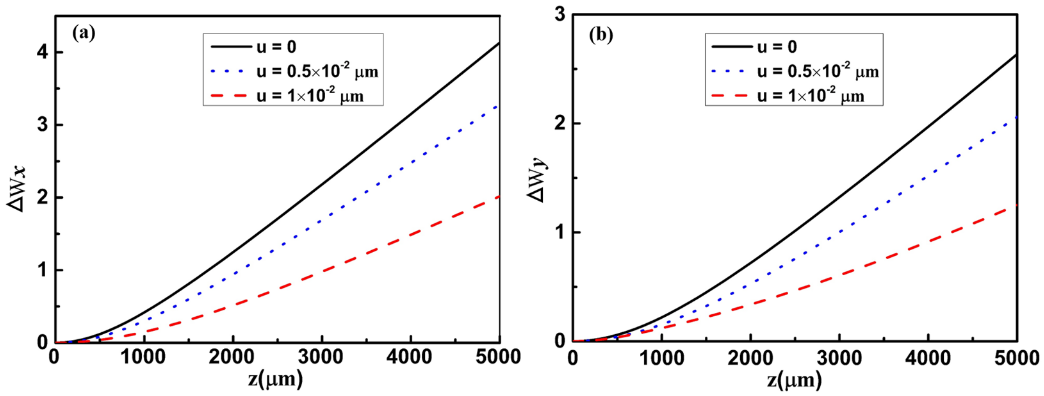


**Figure 8.** The effect of the twist factor on the relative growth rate of (**a**) the effective beam width along the $x$ direction $W_x$, (**b**) the effective beam width along the $y$ direction $W_{y,}$ of THGSM beams propagating in uniaxial crystal.

## 6. Discussion

It is worth discussing and explaining the phenomenon that appears above. Different from the free space and isotropic media, the normalized spectral intensity of THGSM beams propagating in uniaxial crystals present different degrees of stretching which can be seen in Figure 1. As uniaxial crystals are anisotropic crystals, the propagation speed of extraordinary light are different in various directions, while the propagation speed of ordinary light is the same in each direction. The speed when e-light propagates along the direction perpendicular to the crystal optical axis is recorded as $v_e$, which is the maximum speed for the negative uniaxial crystals and the minimum speed for the positive crystals. For negative uniaxial crystals, $n_e/n_o < 1$, the pattern of the normalized spectral intensity and CSD are all stretched in the $y$-axis direction. It is stretched in the $x$-axis direction when $n_e/n_o > 1$, and the degrees of stretching increase in pace with the growth of the ratio.

Analogous to the changing rule of the normalized spectral intensity, the pattern of DOC of the THGSM beams with different twist factors and different beam orders propagating in uniaxial crystals also present different degrees of stretching with the different ratio of $n_e/n_o$. The beam order and the twist factor all affect the distribution of the pattern of the absolute of the normalized spectral intensity and the DOC.

The effective beam width in two directions $W_x$ and $W_y$ of THGSM beams are all affected by different media. When it propagates in uniaxial crystals, both $Wx$ and $Wy$ are affected by the ratio $n_e/n_o$. Additionally, the relative growth rate of the effective beam width is lower when the twist is bigger, as the initial radius are bigger when the twist factor is bigger.

## 7. Conclusions

In this paper, we deduced the concrete representation of the CSD function of THGSM beams propagating in uniaxial crystals orthogonal to the optical axis. Then, we discussed its propagation characteristics, which mainly contain the evolutional properties of the normalized spectral intensity, the DOC, along with the effective beam width. The results show that THGSM beams maintain rotation and self-splitting properties, the same as when propagating in free space and in isotropic media. However, the normalized spectral intensity and DOC present different degrees of stretching. The splitting of the normalized spectral intensity is largely influenced by the twist factor and the beam order. The effective beam width in two directions $Wx$ and $Wy$ are different in different media, and it was found that increasing the twist factor can reduce the relative divergence rate of the beam radius. Therefore, uniaxial crystal can be used to determine whether light beams carry a twist phase or not, which provides one method to modulate the propagation characteristics of THGSM beams, which will be applied in certain fields that require the special properties of THGSM beams.

**Author Contributions:** Writing—original draft preparation, R.L.; writing—review and editing, X.Z.; methodology, R.L. and Y.L.; software, H.S. and J.W.; data curation, H.Z.; supervision, Y.C.; project administration J.Y. and Y.C. All authors have read and agreed to the published version of the manuscript.

**Funding:** This research was funded by the National Key Research and Development Program of China (2022YFA1404800, 2019YFA0705000); the National Natural Science Foundation of China (11904087, 12192254, 12004218, 92250304); the China Postdoctoral Science Foundation (2020M680093, 2022M721992); the Shandong Provincial Natural Science Foundation of China (ZR2020QA067); the Open Fund of the Guangdong Provincial Key Laboratory of Optical Fiber Sensing and Communications (Jinan University: 2022GDSGXCG08); the Open Project of Shandong Key Laboratory of Optics and Photonic Device (K202107); Youth Innovation Program of Universities in Shandong Province (2021KJ091), and Heze University doctoral fund project (XY22BS30).

**Institutional Review Board Statement:** Not applicable.

**Informed Consent Statement:** Not applicable.

**Data Availability Statement:** Data are contained within the article.

**Conflicts of Interest:** The authors declare no conflict of interest.

## References

1. Wolf, E. *Introduction to the Theory of Coherence and Polarization of Light*; Cambridge University: Cambridge, MA, USA, 2007; pp. 174–197.
2. Cai, Y.; Wang, F. Tensor Method for Treating the Propagation of Scalar and Electromagnetic Gaussian Schell-Model Beams: A Review. *Open Opt. J.* **2010**, *4*, 1–20. [CrossRef]
3. Gbur, G. Partially coherent beam propagation in atmospheric turbulence. *J. Opt. Soc. Am. A.* **2014**, *31*, 2038–2045. [CrossRef] [PubMed]
4. Liu, Y.; Zhang, X.; Dong, Z.; Peng, D.; Chen, Y.; Wang, F.; Cai, Y. Robust Far-Field Optical Image Transmission with Structured Random Light Beams. *Phys. Rev. Appl.* **2022**, *17*, 024043. [CrossRef]
5. Peng, D.; Huang, Z.; Liu, Y.; Chen, Y.; Wang, F.; Ponomarenko, S.A.; Cai, Y. Optical coherence encryption with structured random light. *PhotoniX* **2021**, *2*, 6. [CrossRef]
6. Gori, F.; Santarsiero, M. Devising genuine spatial correlation functions. *Opt. Lett.* **2007**, *32*, 3531–3533. [CrossRef]
7. Gori, F.; Ramírez-Sánchez, V.; Santarsiero, M.; Shirai, T. On genuine cross-spectral density matrices. *J. Opt. A Pure Appl. Opt.* **2009**, *11*, 085706. [CrossRef]
8. Sahin, S.; Korotkova, O. Light sources generating far fields with tunable flat profiles. *Opt. Lett.* **2012**, *37*, 2970–2972. [CrossRef] [PubMed]
9. Chen, Y.; Cai, Y. Generation of a controllable optical cage by focusing a Laguerre–Gaussian correlated Schell-model beam. *Opt. Lett.* **2014**, *39*, 2549–2552. [CrossRef]
10. Chen, Y.; Gu, J.; Wang, F.; Cai, Y. Self-splitting properties of a Hermite-Gaussian correlated Schell-model beam. *Phys. Rev. A* **2015**, *91*, 013823. [CrossRef]
11. Ponomarenko, S.A. A class of partially coherent beams carrying optical vortices. *J. Opt. Soc. Am. A* **2001**, *18*, 150–156. [CrossRef]
12. Lajunen, H.; Saastamoinen, T. Propagation characteristics of partially coherent beams with spatially varying correlations. *Opt. Lett.* **2011**, *36*, 4104–4106. [CrossRef] [PubMed]
13. Ma, L.; Ponomarenko, S.A. Optical coherence gratings and lattices. *Opt. Lett.* **2014**, *39*, 6656–6659. [CrossRef] [PubMed]
14. Liang, C.; Zhu, X.; MI, C.; Peng, X.; Wang, F.; Cai, Y.; Ponomarenko, S.A. High-quality partially coherent Bessel beam array generation. *Opt. Lett.* **2018**, *43*, 3188–3191. [CrossRef] [PubMed]
15. Ma, L.; Ponomarenko, S.A. Free-space propagation of optical coherence lattices and periodicity reciprocity. *Opt. Express* **2015**, *23*, 1848–1856. [CrossRef]
16. Lin, R.; Yu, H.; Zhu, X.; Liu, L.; Gbur, G.; Cai, Y.; Yu, J. The evolution of spectral intensity and orbital angular momentum of twisted Hermite Gaussian Schell model beams in turbulence. *Opt. Express* **2020**, *28*, 7152–7164. [CrossRef]
17. Zhang, C.; Zhou, Z.; Xu, H.; Zhou, Z.; Han, Y.; Yuan, Y.; Qu, J. Evolution properties of twisted Hermite Gaussian Schell-model beams in non-Kolmogorov turbulence. *Opt. Express* **2022**, *30*, 4071–4083. [CrossRef]
18. Deng, D.; Yu, H.; Xu, S.; Shao, J.; Fan, Z. Propagation and polarization properties of hollow Gaussian beams in uniaxial crystals. *Opt. Commun.* **2008**, *281*, 202–209. [CrossRef]
19. Zhou, G.; Chen, R.; Chu, X. Propagation of Airy beams in uniaxial crystals orthogonal to the optical axis. *Opt. Express* **2012**, *20*, 2196–2205. [CrossRef]
20. Deng, D.; Chen, C.; Zhao, X.; Li, H. Propagation of an Airy vortex beam in uniaxial crystals. *Appl. Phys. B* **2013**, *110*, 433–436. [CrossRef]
21. Lian, M.; Gu, B.; Zhang, Y.; Rui, G.; He, J.; Zhan, Q.; Cui, Y. Polarization rotation of hybridly polarized beams in a uniaxial crystal orthogonal to the optical axis: Theory and experiment. *J. Opt. Soc. Am. A* **2017**, *34*, 1–6. [CrossRef]

22. Xu, Y.; Zhou, G.; Wang, X. Nonparaxial propagation of Hermite–Laguerre Gaussian beams in uniaxial crystal orthogonal to the optical axis. *Chin. Phys. B* **2013**, *22*, 064101. [CrossRef]
23. Liu, D.; Zhou, Z. Propagation of partially coherent flat topped beams in uniaxial crystals orthogonal to the optical axis. *J. Opt. Soc. Am. A* **2009**, *26*, 924–930. [CrossRef] [PubMed]
24. Zhang, L.; Cai, Y. Statistical properties of a nonparaxial Gaussian Schell-model beam in a uniaxial crystal. *Opt. Express* **2011**, *19*, 13312–13325. [CrossRef] [PubMed]
25. Liu, L.; Peng, X.; Chen, Y.; Guo, L.; Cai, Y. Statistical properties of a radially polarized twisted Gaussian Schell-model beam in a uniaxial crystal. *J. Mod. Optic.* **2016**, *64*, 1–11. [CrossRef]
26. Lu, X.; Shen, Y.; Zhu, X.; Zhao, C.; Cai, Y. Evolution properties of multi-Gaussian Schell model beams propagating in uniaxial crystal orthogonal to the optical axis. *Opt. Appl.* **2016**, *146*, 19–34.
27. Liu, H.; Xia, J.; Lu, Y. Evolution properties of partially coherent standard and elegant Hermite–Gaussian beams in uniaxial crystals. *J. Opt. Soc. Am. A* **2017**, *34*, 2102–2109. [CrossRef]
28. Zhu, Z.; Liu, L.; Wang, F.; Cai, Y. Evolution properties of a Laguerre–Gaussian correlated Schell-model beam propagating in uniaxial crystals orthogonal to the optical axis. *J. Opt. Soc. Am. A* **2015**, *32*, 374–380. [CrossRef]
29. Su, J.; Xu, C.; Xu, H.; Qu, J. Evolution properties of the radially polarized Laguerre-Gaussian-correlated Schell-model beams propagating in uniaxial crystals. *J. Opt. Soc. Am. A* **2020**, *37*, 529–539. [CrossRef]
30. Lin, R.; Chen, M.; Liu, Y.; Zhang, H.; Gbur, G.; Cai, Y.; Yu, J. Measuring refractive indices of a uniaxial crystal by structured light with non-uniform correlation. *Opt. Lett.* **2021**, *46*, 2268–2271. [CrossRef]
31. Ciattoni, A.; Palma, C. Optical propagation in uniaxial crystals orthogonal to the optical axis: Paraxial theory and beyond. *J. Opt. Soc. Am. A* **2003**, *20*, 2163–2171. [CrossRef]
32. Cai, Y.; Chen, Y.; Yu, J.; Liu, X.; Liu, L. Generation of partially coherent beams. *Prog. Opt.* **2017**, *62*, 157–223.
33. Carter, W.H. Spot size and divergence for Hermite Gaussian beams of any order. *Appl. Opt.* **1980**, *19*, 1027–1029. [CrossRef] [PubMed]